

Quantitative Analysis of Stress Relaxation in Polyacrylamide Hydrogels for Mechanobiological Studies

Dawid Łysik^{1*}, Paulina Dziemiańczyk¹, Joanna Mystkowska¹

¹Institute of Biomedical Engineering, Białystok University of Technology, Białystok, Poland

*Corresponding author: Dawid Łysik, Institute of Biomedical Engineering, Białystok University of Technology,
Białystok, Poland, e-mail address: d.lysik@pb.edu.pl

Submitted: 30th April 2025

Accepted: 13th June 2025

ACCEPTED

Abstract

The mechanical environment of the extracellular matrix strongly influences how cells behave — affecting their adhesion, migration, growth, and differentiation. While stiffness has been widely studied, recent research highlights the importance of viscoelasticity, especially the stress relaxation timescale, in how cells sense and respond to their surroundings. According to the widely accepted motor–clutch model, optimal cell spreading occurs when the stress relaxation timescale is similar to the timescale of molecular clutch binding.

Polyacrylamide (PAAm) hydrogels, due to their tunable mechanical properties and bioinert nature, are commonly used as model substrates in mechanobiology. In this study, we investigated how changing the concentrations of crosslinker (N,N'-methylenebisacrylamide) and initiator (ammonium persulfate) affects the viscoelastic behavior of PAAm hydrogels. Using creep–recovery tests and fitting the data to the Standard Linear Solid model, we extracted mechanical parameters and calculated the stress relaxation timescale.

We found that the relaxation timescale increases with crosslinker concentration up to 0.05%, then decreases — suggesting an optimal crosslinking density. At a fixed 0.05% crosslinker, increasing initiator concentration reduced the relaxation timescale, likely due to faster gelation and less organized network formation.

These findings demonstrate how simple adjustments in polymerization parameters can tune hydrogel relaxation behavior for mechanobiological applications.

Keywords

mechanotransduction, stress relaxation time, creep–recovery rheology, motor–clutch model, adhesion dynamics

Introduction

Eukaryotic cells have the ability to sense and respond to mechanical cues from their microenvironment [35]. This process, known as mechanosensing, plays a critical role in essential biological phenomena such as migration, spreading, proliferation, and differentiation — all fundamental for the development, maintenance, and organization of multicellular organisms [26,34]. A central structure in this cellular response is the focal adhesion, a dynamic complex that physically connects the intracellular actin cytoskeleton to the extracellular matrix (ECM), while also acting as a biochemical signaling hub [17,20].

A widely accepted framework for understanding how cells interpret mechanical properties of the ECM is the motor-clutch model [10,17] (fig. 1). In this model, actomyosin contractility generates retrograde flow of actin filaments toward the cell center, while dynamic adhesive bonds (molecular clutches) intermittently connect these filaments to the ECM [6,10]. When clutches engage, the retrograde flow is resisted, allowing the transmission of traction forces to the ECM and promoting membrane protrusion and cell spreading. Key parameters in this system include the clutch binding rate r_{on} , the unbinding rate r_{off} , and the characteristic binding timescale $\tau_b=1/r_{on}$. Meanwhile, the viscoelastic behavior of the ECM can be described by the Standard Linear Solid (SLS) model, which incorporates both elastic (k_0 , k_1) and viscous (η) components. The ECM's ability to relax stress over time is captured by the substrate relaxation timescale $\tau_s=\eta/k_1$ [10].

It has been demonstrated that cell spreading is maximized when the substrate relaxation timescale τ_s is comparable to the clutch binding timescale τ_b [39]. If the ECM relaxes too quickly, forces dissipate before clutches can engage effectively. Conversely, if it relaxes too slowly, the clutches detach before force transmission is optimized [10]. This balance defines a viscoelastic “sweet spot” for efficient mechanotransduction and cellular adhesion.

While much attention has traditionally been placed on the stiffness (Young's modulus) of culture substrates, it is becoming increasingly clear that time-dependent mechanical properties, such as viscosity and stress relaxation, are equally critical in guiding cell behavior [4]. In this context, polyacrylamide (PAAm) hydrogels offer a powerful and tunable platform for controlling ECM mechanics [3,25,28]. Their viscoelastic properties can be precisely adjusted by varying the concentrations of basic components — such as acrylamide, [N,N'-methylenebisacrylamide](#), and [ammonium persulfate](#) [22].

Polyacrylamide is a synthetic, non-toxic polymer known for its water affinity and swelling properties, making it ideal for tissue engineering applications [14]. PAAm can be

easily modified to attain a stiffness range that simulates physiological cell conditions, from several hundred pascals to tens of kilopascals [15]. This attribute positions it as an excellent candidate for exploring the influence of substrate stiffness and chemical signals on cellular behavior [18]. The polymerization process results in polyacrylamide hydrogels forming a predominantly elastic network, with viscosity several orders of magnitude lower than its elasticity [1].

In this study, we aim to investigate whether tuning the formulation of PAAm hydrogels enables control not only over their elastic modulus but also over their viscoelastic characteristics as described by the SLS model. A particular focus is placed on modulating the substrate relaxation timescale τ_s , which is directly relevant to the dynamics of cellular adhesion. Such tailored hydrogels hold potential as cell culture substrates for investigating and influencing mechanosensitive cellular responses [19].

To characterize the mechanical behavior of these materials, rheological measurements were performed on a series of PAAm hydrogels with systematically varied concentrations of BIS and APS (the crosslinker and initiator, respectively). Specifically, creep-recovery tests were carried out to assess the time-dependent deformation response under constant stress and subsequent relaxation. The resulting creep compliance-time profiles were then used to fit the parameters of the SLS Model, allowing for quantitative extraction of viscoelastic parameters such as the instantaneous and equilibrium moduli (k_0 , k_1) and viscosity (η) [2].

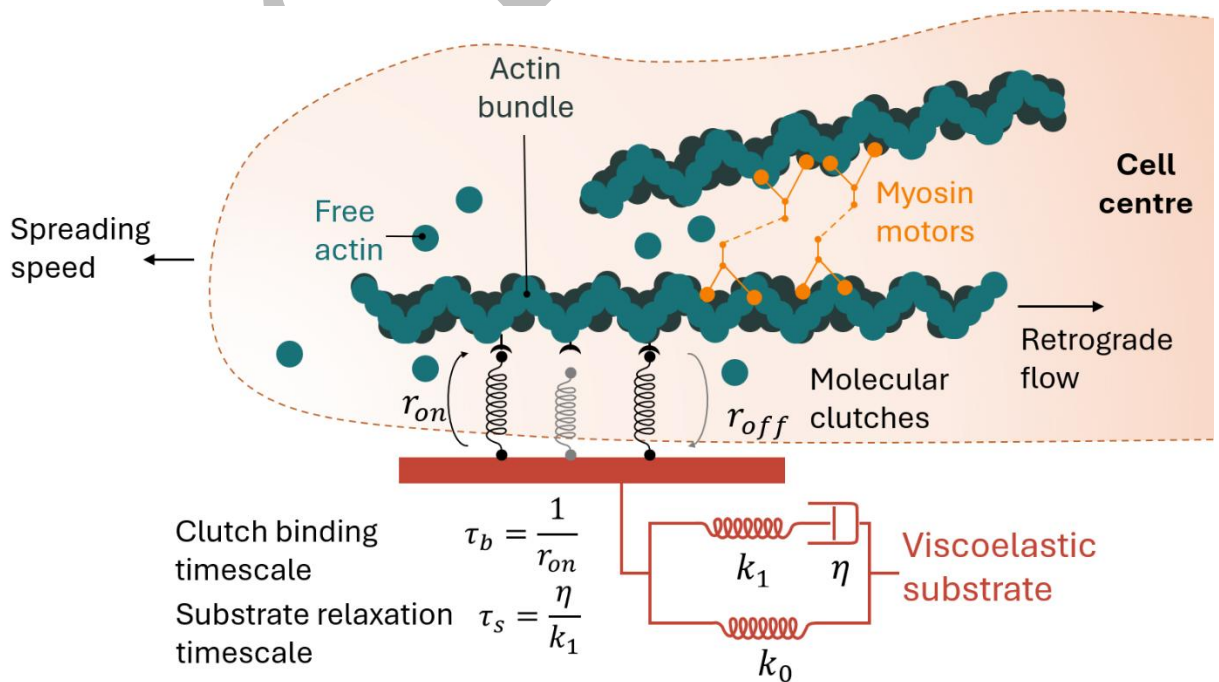


Figure 1. Schematic representation of the molecular clutch model describing force transmission between the actin cytoskeleton and a viscoelastic substrate. Actin filaments undergo retrograde

flow toward the cell center due to contractile forces generated by myosin II motors. Molecular clutches stochastically bind and unbind to the substrate with rates r_{on} and r_{off} , respectively. When bound, clutches transmit force from the actomyosin network to the extracellular matrix (ECM), slowing actin flow and promoting forward protrusion and cell spreading. Adapted from ref. [5].

Materials and methods

Hydrogel Formulation and Polymerization Conditions

The following reagents were purchased from Sigma-Aldrich (Saint Louis, Missouri, USA) and used without further purification: acrylamide (71.08 g/mol), N,N'-methylenebisacrylamide (BIS, 154.17 g/mol), ammonium persulfate (APS, 228.20 g/mol), and N,N,N',N'-tetramethylethylenediamine (TEMED, 116.20 g/mol) (fig. 2). All solutions were prepared using deionized water (Millipore system) and mixed immediately prior to use.

Polyacrylamide (PAAm) hydrogels were synthesized via conventional free radical copolymerization in aqueous solution. A stock solution containing 15% (w/v) acrylamide was prepared using deionized water. To investigate the effect of crosslinking density, various concentrations of N,N'-methylenebisacrylamide (BIS) were added to the acrylamide solution: 0%, 0.025%, 0.05%, 0.075%, and 0.1% (w/v). Polymerization was initiated by the addition of ammonium persulfate (APS) at a constant concentration of 0.5% (w/v) and 0.1% (w/v) TEMED as an accelerator. The reaction mixtures were poured into 35 mm diameter Petri dishes and allowed to polymerize at 4°C for 48 hours. After polymerization, hydrogel discs with a diameter of 20 mm were cut out using a steel punch for further analysis.

To evaluate the effect of initiator concentration on gel properties, a separate set of hydrogels was prepared with a constant BIS concentration of 0.05% (w/v) and varying APS levels: 0.5%, 0.75%, and 1% (w/v), while keeping acrylamide and TEMED concentrations constant at 15% and 0.1%, respectively. All hydrogels were polymerized under identical conditions and stored at 4°C until further analysis.

Tables 1 and 2 summarize the formulations used in each series.

Table 1. Compositions of PAAm hydrogels with varying concentrations of N,N'-methylenebisacrylamide (BIS) crosslinker.

Sample	Acrylamide (%)	N,N'-methylenebisacrylamide (%)	APS (%)	TEMED (%)
PAAm-0 BIS	15	0	0.5	0.1
PAAm-0.025 BIS	15	0.025	0.5	0.1

PAAm-0.05 BIS	15	0.05	0.5	0.1
PAAm-0.075 BIS	15	0.075	0.5	0.1
PAAm-0.1 BIS	15	0.1	0.5	0.1

Table 2. Compositions of PAAm hydrogels with varying concentrations of ammonium persulfate (APS) initiator.

Sample	Acrylamide (%)	BIS (%)	Ammonium persulfate (%)	TEMED (%)
PAAm-0.5 APS	15	0.05	0.5	0.1
PAAm-0.75 APS	15	0.05	0.75	0.1
PAAm-1 APS	15	0.05	1	0.1

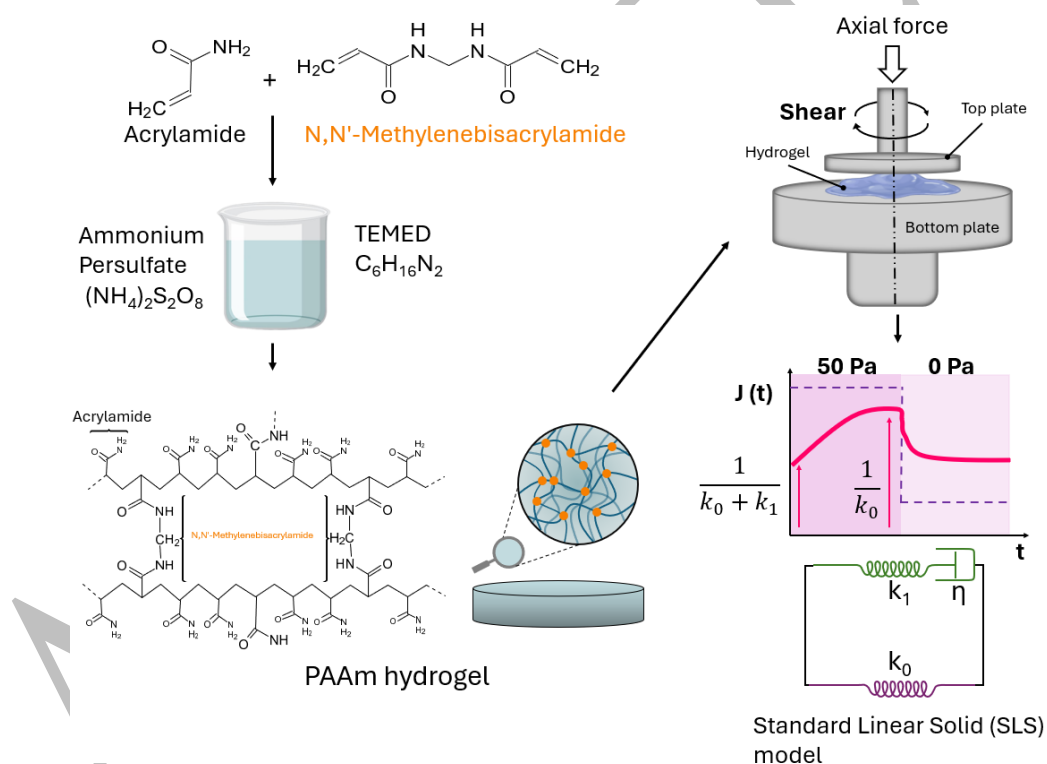


Figure 2. Schematic representation of polyacrylamide (PAAm) hydrogel synthesis and rheological characterization using the Standard Linear Solid (SLS) model. Acrylamide was polymerized in the presence of BIS as a crosslinker and APS as an initiator, with TEMED as an accelerator. The resulting hydrogel network consists of covalently crosslinked polymer chains. Rheological measurements were performed using a parallel plate geometry under oscillatory shear or creep-recovery conditions. The viscoelastic response was analyzed by fitting the experimental data to the Standard Linear Solid (SLS) model, characterized by a combination of

springs (k_0 , k_1) and a dashpot (η), allowing extraction of mechanical parameters and substrate relaxation behavior.

Creep–Recovery Measurements

The bulk rheological properties of the hydrogels were evaluated using a HAAKE RheoStress 6000 rotational rheometer (Thermo Fisher Scientific, USA) equipped with a plate-to-plate geometry. In this configuration, the upper rotating plate had a diameter of 20 mm, while the lower stationary plate measured 60 mm and featured a grid surface to prevent sample slippage. The tests were carried out at a controlled temperature of 21°C (fig. 2).

Each hydrogel sample was loaded onto the bottom plate and compressed with a normal force of 2 N to ensure contact. Creep–recovery experiments were performed by applying a constant shear stress (τ) of 50 Pa for 100 seconds (creep phase), followed by complete stress removal for another 100 seconds (recovery phase). During both phases, the time-dependent strain ($\gamma(t)$) of the sample was continuously recorded. **For each hydrogel formulation, three independent samples were tested.**

For each measurement, the rheometer software was used to calculate the creep compliance $J(t)$, defined as the ratio of strain to applied stress (1):

$$J(t) = \frac{\gamma(t)}{\tau} \quad (1)$$

where $\gamma(t)$ is the strain recorded as a function of time and τ is the constant applied stress during the creep phase.

Quantitative Modeling of Viscoelastic Response

The time-dependent creep compliance data obtained from rheological measurements were analyzed using OriginPro 2024 (OriginLab Corporation, USA). Nonlinear curve fitting was performed using the Orthogonal Distance Regression (ODR) algorithm, providing improved accuracy for experimental data fitting.

Two separate models were used to fit different phases of the test:

- The Standard Linear Solid (SLS) model was applied to fit the creep phase [2], allowing the extraction of viscoelastic parameters including the instantaneous modulus (k_0), equilibrium modulus (k_1), and viscosity (η) (2):

$$J(t) = \left(\frac{1}{k_0 + k_1} \right) + \left(\frac{1}{k_0} - \frac{1}{k_1} \right) \left(1 - \exp \left(-t \left(\frac{k_0 k_1}{\eta (k_0 + k_1)} \right) \right) \right) \quad (2)$$

- The Weibull distribution function was used to describe the recovery phase after stress removal [38], enabling a better characterization of the relaxation behavior beyond the linear viscoelastic regime (3):

$$J(t) = J_v \left(\exp \left(- \left(\frac{t - t_0}{\lambda} \right)^\beta \right) \right) + J_p \quad (3)$$

In this expression, $J(t)$ represents the time-dependent creep compliance, and t_0 is the time at which the stress is removed (i.e., the beginning of the recovery phase). The parameter J_v corresponds to the viscoelastic compliance amplitude, which reflects the magnitude of reversible deformation. The term λ is the characteristic timescale of the relaxation process, with larger values indicating slower recovery. The exponent β , known as the shape parameter, defines the curvature of the response: values of $\beta > 1$ indicate a fast initial relaxation followed by a slower decay, while $\beta < 1$ indicates a gradual onset of relaxation. Finally, J_p accounts for the permanent deformation component that remains unrecovered, often associated with irreversible structural changes in the hydrogel network.

Spectroscopic Analysis by FTIR

Fourier transform infrared (FTIR) spectroscopy was used to characterize the chemical bonds present in the PAAm hydrogels. Spectra were recorded using an Alpha II FTIR spectrometer (Bruker, Germany) equipped with a diamond attenuated total reflectance (ATR) accessory, operating over the spectral range of 4000–400 cm^{-1} , with a resolution of 2 cm^{-1} . The hydrogels were measured in direct contact with the diamond ATR crystal.

Results

Creep–Recovery Behavior as a Function of Crosslinker and Initiator Concentration

The viscoelastic response of polyacrylamide (PAAm) hydrogels was investigated using creep–recovery measurements under constant shear stress. Figure 3 shows the time-dependent creep compliance curves for hydrogels with varying concentrations of crosslinker (BIS) and initiator (APS). All samples were subjected to a constant shear stress of 50 Pa for 100 seconds (creep phase), followed by a 100-second recovery phase at 0 Pa.

In Figure 3(a), increasing BIS concentration (0–0.1%) resulted in a pronounced reduction in creep compliance, indicating greater structural rigidity with higher crosslinking. The maximum creep compliance at the end of the creep phase (100 s) decreased from 0.042 Pa^{-1} for PAAm-0 BIS to 0.0012 Pa^{-1} for PAAm-0.05 BIS, confirming a nearly order-of-magnitude

reduction in deformability. Notably, the 0.05% BIS hydrogel exhibited the lowest compliance of all tested samples, including those with even higher BIS content, suggesting the presence of an optimal crosslinking density at this concentration.

Interestingly, beyond this threshold (0.075% and 0.1% BIS), creep compliance values slightly increased to 0.0034 and 0.0033 Pa⁻¹, respectively. This non-monotonic behavior may result from an oversaturation of crosslinker molecules in the polymer matrix, which, due to limited availability of acrylamide chains, may no longer contribute effectively to the network. Instead, excess BIS could introduce dangling ends or microstructural irregularities, thus reducing the network's mechanical efficiency.

A one-way ANOVA performed on creep compliance values at 100 seconds indicated that 0% BIS differed significantly from all other formulations ($p < 0.01$), while 0.025% BIS differed from 0.05% BIS ($p < 0.05$), and showed a trend toward significance versus 0.075% and 0.1% BIS ($p < 0.1$). No significant differences were found among the remaining samples.

Figure 3(b) illustrates the effect of varying APS concentration (0.5–1%) at a fixed BIS level of 0.05%. In contrast to the BIS trend, creep compliance increased monotonically with APS content, reaching values of 0.0012, 0.0022, and 0.0038 Pa⁻¹ for 0.5%, 0.75%, and 1% APS, respectively. These results indicate that higher initiator levels, although accelerating polymerization, may lead to rapid chain termination and reduced network homogeneity.

Dashed lines in both graphs show model fits based on the SLS model. The accuracy of these fits supports the suitability of the SLS framework for describing PAAm hydrogel mechanics under creep conditions. The resulting parameters are discussed in the following section.

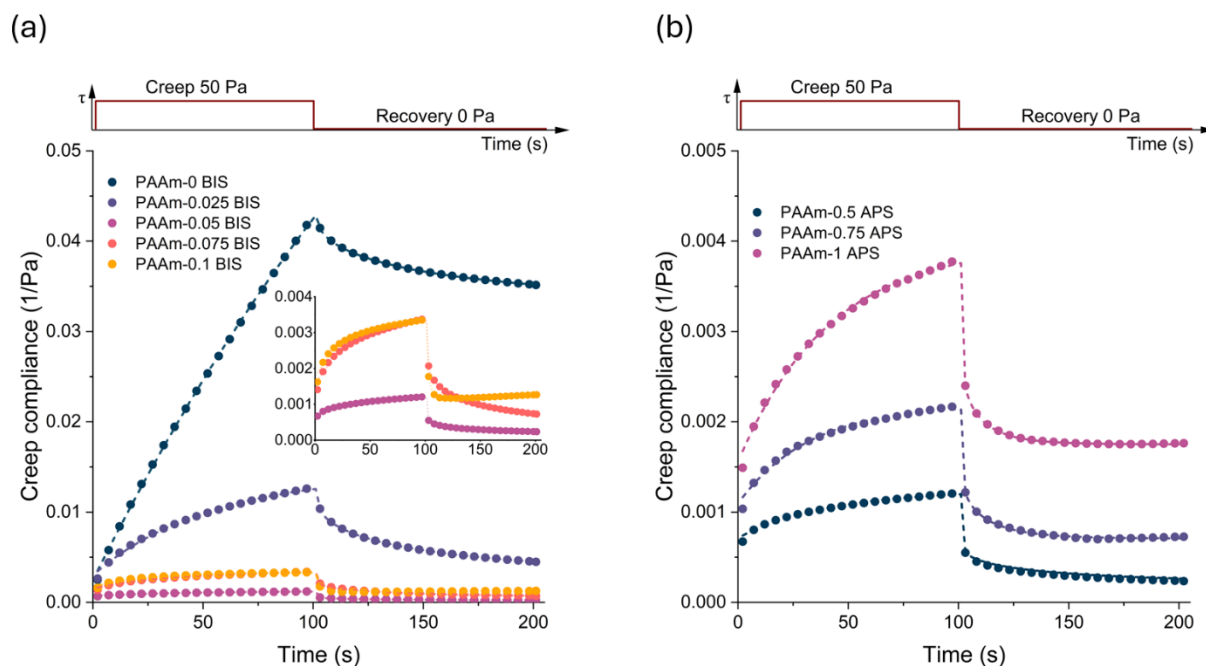


Figure 3. Creep compliance of 15% polyacrylamide (PAAm) hydrogels as a function of crosslinker and initiator concentration: (a) Creep–recovery curves for PAAm hydrogels with varying BIS content, and (b) with varying APS content, measured under constant shear stress of 50 Pa (creep) and 0 Pa (recovery). The red trace above each plot shows the applied stress profile. Dashed lines represent SLS model fits. The inset in (a) highlights overlapping curves for PAAm-0.05%, 0.075%, and 0.1% BIS.

Determination of SLS Model Parameters and Relaxation Timescale

To quantitatively describe the time-dependent mechanical response of PAAm hydrogels, creep–recovery data were fitted to the SLS model (2). The obtained parameters included the instantaneous modulus (k_0), equilibrium modulus (k_1), and viscosity (η). Based on these values, the hydrogel relaxation timescale was calculated using the formula $\tau_s = \eta/k_1$, representing the characteristic time required for stress dissipation.

As shown in Table 3 and Figure 4(a), the PAAm-0.05 BIS hydrogel exhibited the highest viscoelastic stiffness, with fitted parameters of $k_0=573$ Pa, $k_1=823$ Pa, and $\eta=14066$ Pa·s. The resulting substrate relaxation timescale reached a maximum of 17.10 s, significantly higher than values observed for both lower and higher BIS concentrations. For comparison, the BIS-free sample (PAAm-0 BIS) showed a low modulus ($k_0=8$ Pa), negligible equilibrium stiffness ($k_1=388$ Pa), and minimal viscosity ($\eta=1947$ Pa·s), yielding a relaxation time of just 5.01 s, confirming its weak, fluid-like character.

Interestingly, the relaxation time for 0.075% and 0.1% PAAm-BIS decreased to 12.71 s and 10.27 s, respectively, despite the higher crosslinker content (fig. 4c). This reinforces the

conclusion that 0.05% BIS represents a critical crosslinking point, beyond which further addition of BIS does not improve — and may even deteriorate — network efficiency, likely due to excess unreacted BIS leading to heterogeneities.

In the second series (fig. 4b, tab. 4), increasing the APS concentration from 0.5% to 1% led to a progressive decrease in all SLS parameters. At 0.5% APS, the fitted values were $k_0 = 573$ Pa, $k_1 = 823$ Pa, and $\eta = 14066$ Pa·s, identical to the BIS-optimum, with a τ_s of 17.10 s (fig. 4d). However, at 1% APS, these values dropped to $k_0 = 211$ Pa, $k_1 = 429$ Pa, and $\eta = 5873$ Pa·s, yielding a shorter relaxation time of 13.67 s (fig. 4d). This reduction may be attributed to more rapid radical generation, leading to shorter polymer chains and less uniform network formation.

Overall, the results clearly indicate that the mechanical integrity and relaxation dynamics of PAAm hydrogels are strongly dependent on both BIS and APS concentrations. Notably, the combination of 0.05% BIS and 0.5% APS yielded the most mechanically robust and slowly relaxing hydrogel, as reflected by the peak τ_s , highest elastic moduli, and greatest viscosity among all tested formulations.

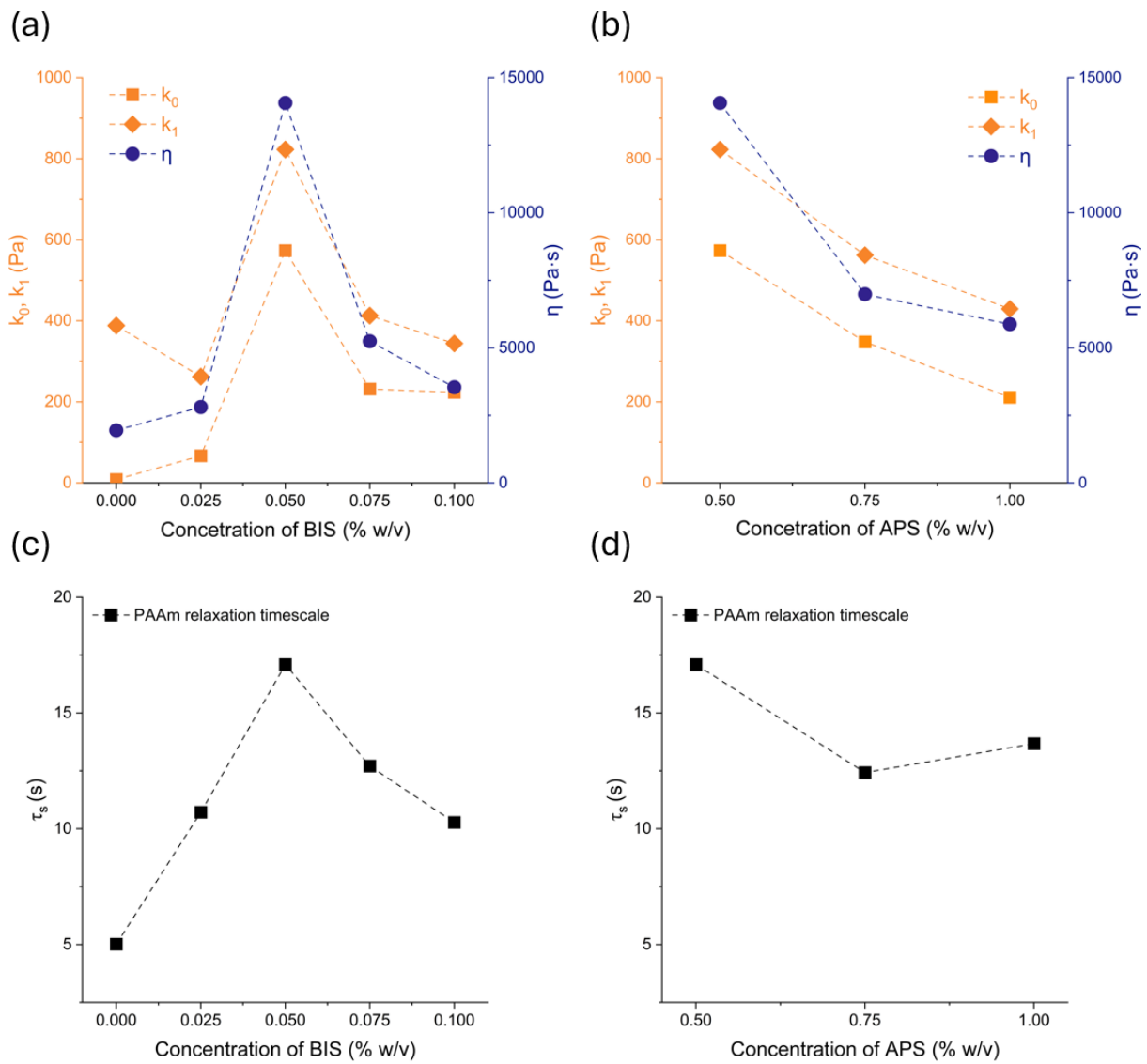


Figure 4. Viscoelastic parameters of polyacrylamide hydrogels fitted using the Standard Linear Solid (SLS) model and derived substrate relaxation timescale: (a, b) Parameters of the SLS model, instantaneous modulus k_0 , equilibrium modulus k_1 , and viscosity η , as a function of: (a) BIS (N,N'-methylenebisacrylamide) concentration and (b) APS (ammonium persulfate) concentration; (c, d) Substrate relaxation timescale $\tau_s = \eta/k_1$ calculated from the fitted parameters as a function of crosslinker BIS and APS concentration, respectively.

Table 3. Fitted viscoelastic parameters of PAAm hydrogels with varying concentrations of N,N'-methylenebisacrylamide (BIS) crosslinker. R^2 values exceeded 0.99 for all formulations, except PAAm-0.1% BIS (0.98 for creep, 0.86 for recovery).

		PAAm-0 BIS	PAAm-0.025 BIS	PAAm-0.05 BIS	PAAm-0.075 BIS	PAAm-0.1 BIS
Creep	k_0	8	67	573	232	224
	k_1	388	262	823	413	344

	η	1947	2809	14066	5245	3536
	λ	55.54	49.20	34.89	37.70	2.67
Recovery	β	0.66	0.64	0.58	0.60	1.29
	J_p	0.0333	0.0029	0.0002	0.0005	0.0012
	J_v	0.0083	0.0076	0.0004	0.0016	0.0006

Table 4. Fitted viscoelastic parameters of PAAm hydrogels with varying concentrations of ammonium persulfate (APS) initiator. The fittings for both creep and recovery models yielded R^2 values greater than 0.99 for all formulations.

		PAAM-0.5 APS	PAAM-0.75 APS	PAAM-1 APS
Creep	k_0	573	348	211
	k_1	823	562	429
	η	14066	6987	5873
Recovery	λ	34.89	11.44	8.99
	β	0.58	0.78	0.79
	J_p	0.0002	0.0007	0.0018
	J_v	0.0004	0.0005	0.0006

Analysis of Recovery Dynamics Using the Weibull Distribution

The recovery phase of the creep–recovery experiments was analyzed by fitting the compliance data to the Weibull distribution (3). The extracted parameters — J_v , J_p , λ , and β — offer insight into both reversible and irreversible components of deformation, as well as the temporal characteristics of the recovery process.

The viscoelastic compliance amplitude J_v reflects the amount of strain that is recoverable after stress removal. The PAAm-0.05 BIS hydrogel exhibited the lowest J_v (0.0004 Pa⁻¹), indicating the most efficient elastic recovery. This result aligns with its low creep compliance and high stress relaxation time τ_s , confirming a well-structured, resilient network. In contrast, the BIS-free hydrogel showed a markedly higher J_v (0.0083 Pa⁻¹), consistent with its predominantly viscous, non-recoverable character.

Permanent deformation was quantified via J_p , the compliance remaining after full recovery. Again, the 0.05% BIS sample had the lowest J_p (0.0002 Pa⁻¹), suggesting nearly

complete reversibility, whereas the BIS-free sample displayed significant residual strain ($J_p = 0.0333 \text{ Pa}^{-1}$), indicative of its fluid-like nature.

The recovery time scale λ , derived from the Weibull fit, ranged from 2.67 to 55.54 seconds. The BIS-free formulation had the longest λ , reflecting slow and incomplete recovery typical of uncrosslinked, viscous systems. Samples with BIS exhibited progressively shorter λ values as BIS content increased, indicating faster recovery kinetics. However, this trend did not follow the same pattern as the stress relaxation time τ_s , or the equilibrium modulus k_1 , both of which peaked at 0.05% BIS. This suggests that λ captures different aspects of the recovery process, potentially influenced by network reorganization beyond what is described by classical viscoelastic models.

The shape parameter β ranged from 0.58 to 1.29. A β value below 1, observed for the 0.05% BIS sample ($\beta = 0.58$), points to stretched exponential behavior and a broad distribution of relaxation times, often associated with structural heterogeneity. Conversely, $\beta > 1$ — as seen in the 0.1% BIS sample ($\beta = 1.29$) — suggests a more rapid, uniform recovery. Notably, this maximum β did not coincide with the peak in τ_s , reinforcing that β and τ_s describe different features of time-dependent mechanical behavior. While β characterizes the shape of the recovery profile, τ_s reflects the overall timescale of stress dissipation. Thus, although 0.1% BIS may enable faster and more synchronized recovery, the 0.05% BIS hydrogel remains optimal in resisting sustained deformation.

Overall, these results confirm that the PAAm-0.05 BIS formulation exhibits the most balanced recovery behavior — combining low residual strain, strong elastic return, and a prolonged yet efficient relaxation response. These findings are consistent with the trends observed during the creep phase and reinforce the presence of an optimal crosslinking concentration at 0.05% BIS.

FTIR Spectra and Chemical Characterization of the Hydrogel Network

The FTIR spectra of PAAm-BIS and PAAm-APS hydrogels are presented in figure 5. A broad and intense band observed in the region $3700\text{--}3000 \text{ cm}^{-1}$ is attributed to O–H stretching vibrations, which indicates the presence of hydrogen bonding, likely associated with absorbed water or hydroxyl groups. This band may also partially overlap with N–H stretching vibrations from primary amide groups ($-\text{NH}_2$) [29].

Characteristic peaks related to the amide I band are found at 1691 cm^{-1} , 1603 cm^{-1} , and $1585\text{--}1591 \text{ cm}^{-1}$, corresponding to the C=O stretching vibrations of the amide groups [13]. The

signals at 1585–1591 cm^{-1} may also be influenced by N–H in-plane bending in the CONH_2 moiety [30].

Additional absorption peaks at 1417 cm^{-1} and in the range 1290–1294 cm^{-1} are associated with C–N stretching (amide III) and C–H bending vibrations of the acrylamide backbone [27,32]. The presence of these peaks confirms the successful polymerization of acrylamide and incorporation of amide functionalities in the hydrogel network.

A small band near 1011–1079 cm^{-1} is observed in several spectra, which may correspond to in-plane rocking of $-\text{NH}_2$ or C–O stretching from side chain interactions, depending on the degree of crosslinking and hydration [7].

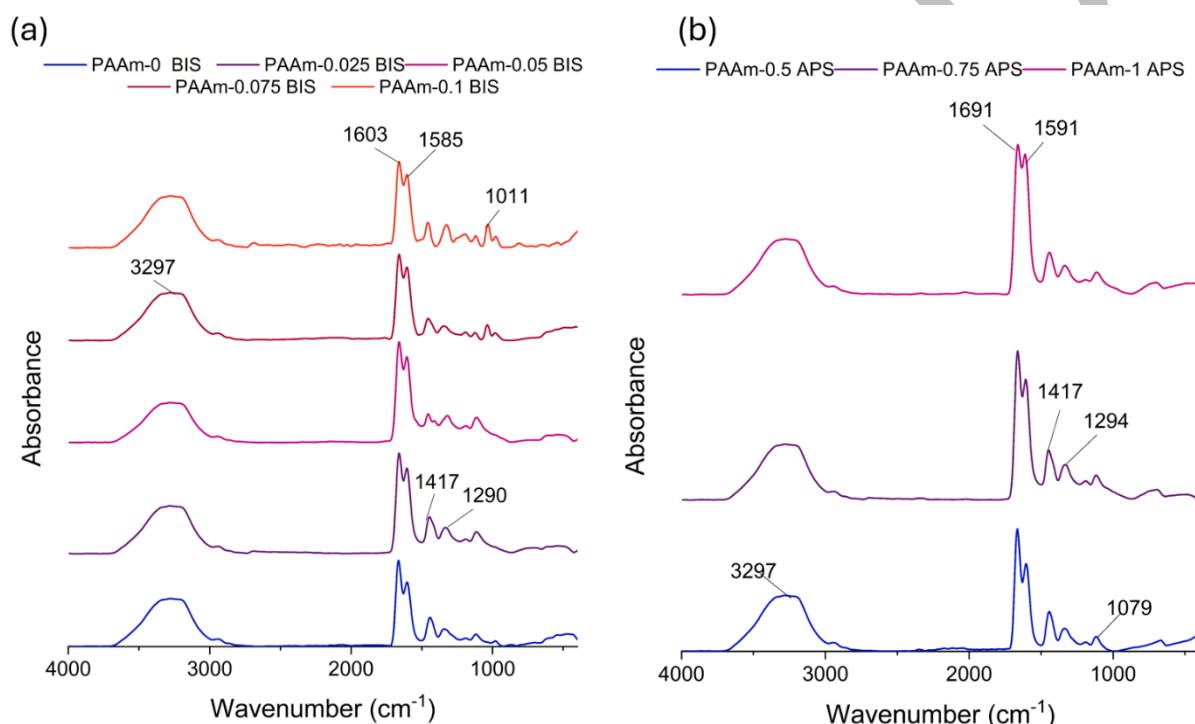


Figure 5. FTIR spectra of polyacrylamide (PAAm) hydrogels with varying concentrations of crosslinker and initiator: (a) Spectra of hydrogels synthesized with 15% acrylamide and increasing concentrations of N,N'-methylenebisacrylamide (BIS); (b) Spectra of hydrogels with constant BIS content (0.05%) and varying concentrations of ammonium persulfate (APS).

Discussion

Polyacrylamide (PAAm) hydrogels are widely used as model substrates in mechanobiology due to their tunable mechanical properties and inert chemistry [21,24,25]. Their mechanical versatility makes them an essential platform for studying how cells interact with their environment.

In mechanobiology, stiffness is often used to describe how resistant a material is to deformation under force. While frequently linked to the elastic modulus, stiffness is system-dependent and reflects both material and geometric properties, as well as the timescale of loading [15]. Cells sense stiffness through focal adhesions by transmitting cytoskeletal forces to the substrate. Stiffer matrices resist deformation and enable higher tension buildup, promoting spreading, migration, proliferation, and differentiation. One of the most consistent findings is that cell area increases with substrate stiffness [29]. Fibroblasts, stem cells, and epithelial cells all spread more extensively on stiffer substrates, often forming stronger adhesions and more pronounced stress fibers. Stiffer substrates provide resistance to contractile forces, stabilizing adhesion sites and enhancing mechanotransduction.

Cell volume has also been observed to decrease on stiffer substrates, correlating with increased spread area and intracellular crowding [16]. This is linked to water efflux and possibly to enhanced nuclear and cytoskeletal tension [11]. Moreover, cells modulate their own stiffness in response to matrix mechanics. Mesenchymal stem cells and other lineages increase cortical stiffness on stiffer substrates, independent of stress fiber formation [9].

Native extracellular matrices and many synthetic hydrogels exhibit viscoelasticity or viscoplasticity. Studies show that cells spread more and generate higher forces on nonlinear, strain-stiffening matrices, such as fibrin, even when low-strain stiffness matches that of elastic controls [12]. These dynamic mechanical cues also influence other cellular processes. Matrix stiffness has been shown to regulate metabolic activity and proliferation. Cells on stiffer matrices often exhibit increased glucose uptake, ATP production, and mitochondrial activity [36]. Proliferation rates also increase with stiffness, with optimal growth occurring at intermediate moduli for certain cell types [33], often mediated through mechanotransductive pathways such as focal adhesion kinase activation [37].

Importantly, stem cell differentiation is also regulated by substrate stiffness, with maximal efficiency occurring when the mechanical properties of the matrix match those of the target tissue. For example, soft substrates favor neurogenesis, intermediate stiffness promotes myogenesis, and stiffer matrices support osteogenesis [23]. Therefore, mimicking tissue-specific stiffness profiles is essential for directing cell fate in vitro.

However, it has become increasingly clear that stiffness alone does not fully capture the mechanical environment sensed by cells. Viscoelasticity, and in particular the stress relaxation timescale, plays a crucial role in mechanotransduction. According to theoretical and experimental work [10], cell spreading is optimized when the substrate relaxation timescale is comparable to or slightly greater than the clutch binding timescale, typically on the order of 1–

10 seconds for most cell types. If the substrate relaxes too quickly (i.e., $\tau_s < \tau_b$), mechanical signals dissipate before adhesion complexes can mature, leading to poor mechanosensing. Conversely, excessively high τ_s values can mimic overly rigid substrates, which may hinder clutch engagement or cause saturation of adhesion reinforcement.

In this study, we demonstrated that by systematically varying the concentrations of crosslinker (BIS) and initiator (APS), it is possible to control the viscoelastic properties of PAAm hydrogels, specifically the stress relaxation timescale τ_s . Creep–recovery experiments combined with SLS modeling allowed us to extract key mechanical parameters and calculate across different formulations. We observed that increasing the BIS concentration led to a rise in τ_s , peaking at 0.05% BIS with a relaxation time of approximately 17 s, compared to ~5 s in gels without BIS. Further increases in BIS resulted in a decrease in τ_s , suggesting the existence of an optimal crosslinking density where the network structure is most effective in resisting stress relaxation. At a fixed 0.05% BIS concentration, increasing the initiator (APS) content led to a progressive decrease in τ_s , likely due to faster polymerization kinetics that promote rapid but less organized network formation.

Recent modeling work by Solowiej-Wedderburn and Dunlop [31] emphasized that spatial patterning of cell adhesions critically affects the effective stiffness experienced by the cell. Their results suggest that the same substrate can be sensed as stiffer or softer depending on adhesion distribution. On stiff substrates, growing and elongating focal adhesions is energetically favorable, consistent with experimental findings of focal adhesion maturation. In contrast, on soft substrates, focal adhesion growth is energetically discouraged. These insights complement the motor–clutch model by incorporating geometric and energetic factors into cell–matrix interaction paradigms.

Our findings partially align with observations by Charrier et al. [4], who engineered viscoelastic PAAm hydrogels with independently tunable elastic (G') and viscous (G'') moduli. In their study, hydrogels were synthesized by combining crosslinked PAAm with linear, uncrosslinked PAAm chains, enabling independent control of the viscous component while maintaining constant elasticity. They focused on dynamic mechanical analysis, distinguishing between the elastic and viscous contributions to the complex modulus. By regulating G'' at a fixed G' , they demonstrated that increased viscous dissipation alone, without changes in elastic stiffness, suppressed cell spreading, stiffening, and osteogenic differentiation. Our study, in contrast, focused on determining the stress relaxation timescale through creep–recovery measurements, which is closely related to energy dissipation during deformation. Importantly, the method of hydrogel preparation developed by Pogoda et al. [24] can be combined with our

straightforward approach to determining τ_s , allowing independent tuning of both elastic and viscous parameters while maintaining the ability to characterize the overall viscoelastic response in a simple and accessible manner.

Our work provides a practical strategy for tuning the stress relaxation timescale of PAAm hydrogels via simple adjustments of polymerization parameters. Including viscoelastic characterization, in addition to standard stiffness measurements, allows for a more complete mechanical profile and enhances the physiological relevance of in vitro models for studying cellular mechanotransduction. This study demonstrates how the viscoelastic properties of PAAm hydrogels can be tuned by adjusting the concentrations of crosslinker and initiator, and how these modifications influence time-dependent mechanical parameters relevant to cell–matrix interactions.

Conclusions

This study presents a systematic investigation into how the viscoelastic properties of polyacrylamide hydrogels can be modulated by altering the concentrations of crosslinker and initiator, with a focus on the resulting substrate relaxation timescale (τ_s). Using creep–recovery rheology and fitting to the SLS model, the authors identify an optimal formulation, 0.05% BIS and 0.5% APS, that yields maximal stiffness and the longest τ_s , essential for effective force transmission in cell–matrix interactions. These findings provide a practical approach for designing biomimetic materials with tunable mechanical cues relevant to mechanotransduction, emphasizing that both elastic and time-dependent properties must be considered in engineering substrates for cell culture.

Funding

This scientific work was realized in the frame of work, No. W/WM-IIB/3/2023, and financed from the research funds of the Ministry of Science and Higher Education, Poland.

Bibliography

1. Basu A, Wen Q, Mao X, Lubensky TC, Janmey PA, Yodh AG. Nonaffine Displacements in Flexible Polymer Networks. *Macromolecules*. 2011, 44(6):1671–9.
2. Bonfanti A, Kaplan JL, Charras G, Kabla A. Fractional viscoelastic models for power-law materials. *Soft Matter*. 2020, 16(26):6002–20.

3. Charrier EE, Pogoda K, Li R, Park CY, Fredberg JJ, Janmey PA. A novel method to make viscoelastic polyacrylamide gels for cell culture and traction force microscopy. *APL Bioeng.* 2020, 4(3):036104.
4. Charrier EE, Pogoda K, Wells RG, Janmey PA. Control of cell morphology and differentiation by substrates with independently tunable elasticity and viscous dissipation. *Nat Commun.* 2018, 9(1):449.
5. Chaudhuri O. Effects of extracellular matrix viscoelasticity on cellular behaviour.
6. Chaudhuri O, Cooper-White J, Janmey PA, Mooney DJ, Shenoy VB. The impact of extracellular matrix viscoelasticity on cellular behavior. 2021, .
7. Cong H, Wang P, Yu S. Highly Elastic and Superstretchable Graphene Oxide/Polyacrylamide Hydrogels. *Small.* 2014, 10(3):448–53.
8. Engler AJ, Richert L, Wong JY, Picart C, Discher DE. Surface probe measurements of the elasticity of sectioned tissue, thin gels and polyelectrolyte multilayer films: Correlations between substrate stiffness and cell adhesion. *Surf Sci.* 2004, 570(1–2):142–54.
9. Engler AJ, Sen S, Sweeney HL, Discher DE. Matrix Elasticity Directs Stem Cell Lineage Specification. *Cell.* 2006, 126(4):677–89.
10. Gong Z, Szczesny SE, Caliari SR, Charrier EE, Chaudhuri O, Cao X, et al. Matching material and cellular timescales maximizes cell spreading on viscoelastic substrates. *Proc Natl Acad Sci.* 2018, 115(12).
11. Guo M, Pegoraro AF, Mao A, Zhou EH, Arany PR, Han Y, et al. Cell volume change through water efflux impacts cell stiffness and stem cell fate. *Proc Natl Acad Sci.* 2017, 114(41).
12. Hall MS, Alisafaei F, Ban E, Feng X, Hui CY, Shenoy VB, et al. Fibrous nonlinear elasticity enables positive mechanical feedback between cells and ECMs. *Proc Natl Acad Sci.* 2016, 113(49):14043–8.
13. Jafari A, Amirsadeghi A, Hassanajili S, Azarpira N. Bioactive antibacterial bilayer PCL/gelatin nanofibrous scaffold promotes full-thickness wound healing. *Int J Pharm.* 2020, 583:119413.
14. Jafari A, Hassanajili S, Ghaffari F, Azarpira N. Modulating the physico-mechanical properties of polyacrylamide/gelatin hydrogels for tissue engineering application. *Polym Bull.* 2022, 79(3):1821–42.
15. Janmey PA, Fletcher DA, Reinhart-King CA. Stiffness Sensing by Cells. *Physiol Rev.* 2020, 100(2):695–724.
16. Karim A, Hall AC. Chondrocyte Morphology in Stiff and Soft Agarose Gels and the Influence of Fetal Calf Serum. *J Cell Physiol.* 2017, 232(5):1041–52.
17. Kechagia JZ, Ivaska J, Roca-Cusachs P. Integrins as biomechanical sensors of the microenvironment. *Nat Rev Mol Cell Biol.* 2019, 20(8):457–73.

18. Lee JP, Kassianidou E, MacDonald JJ, Francis MB, Kumar S. N-terminal specific conjugation of extracellular matrix proteins to 2-pyridinecarboxaldehyde functionalized polyacrylamide hydrogels. *Biomaterials*. 2016, 102:268–76.
19. Lu P. Harnessing the potential of hydrogels for advanced therapeutic applications: current achievements and future directions. *Signal Transduct Target Ther*. 2024, .
20. Mavrakis M, Juanes MA. The compass to follow: Focal adhesion turnover. *Curr Opin Cell Biol*. 2023, 80:102152.
21. Milos F, Del Campo A. Polyacrylamide Hydrogels as Versatile Biomimetic Platforms to Study Cell-Materials Interactions. *Adv Mater Interfaces*. 2024, 11(34):2400404.
22. Narasimhan BN, Horrocks MS, Malmström J. Hydrogels with Tunable Physical Cues and Their Emerging Roles in Studies of Cellular Mechanotransduction. *Adv NanoBiomed Res*. 2021, 1(10):2100059.
23. Nasrollahi S, Walter C, Loza AJ, Schimizzi GV, Longmore GD, Pathak A. Past matrix stiffness primes epithelial cells and regulates their future collective migration through a mechanical memory. *Biomaterials*. 2017, 146:146–55.
24. Pogoda K, Charrier E, Janmey P. A Novel Method to Make Polyacrylamide Gels with Mechanical Properties Resembling those of Biological Tissues. *BIO-Protoc*. 2021, 11(16).
25. Protick FK, Amit SK, Amar K, Nath SD, Akand R, Davis VA, et al. Additive Manufacturing of Viscoelastic Polyacrylamide Substrates for Mechanosensing Studies. *ACS Omega*. 2022, 7(28):24384–95.
26. Sala S, Caillier A, Oakes PW. Principles and regulation of mechanosensing. *J Cell Sci*. 2024, 137(18):jcs261338.
27. Samanta HS, Ray SK. Synthesis, characterization, swelling and drug release behavior of semi-interpenetrating network hydrogels of sodium alginate and polyacrylamide. *Carbohydr Polym*. 2014, 99:666–78.
28. Shi L, Lim JY, Kam LC. Substrate stiffness enhances human regulatory T cell induction and metabolism. *Biomaterials*. 2023, 292:121928.
29. Shi Y, Li J, Xiong D, Li L, Liu Q. Mechanical and tribological behaviors of PVA / PAAM double network hydrogels under varied strains as cartilage replacement. *J Appl Polym Sci*. 2021, 138(16):50226.
30. Sobhanian P, Khorram M, Hashemi SS, Mohammadi A. Development of nanofibrous collagen-grafted poly (vinyl alcohol)/gelatin/alginate scaffolds as potential skin substitute. *Int J Biol Macromol*. 2019, 130:977–87.
31. Solowiej-Wedderburn J, Dunlop CM. Sticking around: Cell adhesion patterning for energy minimization and substrate mechanosensing. *Biophys J*. 2022, 121(9):1777–86.
32. Sternik D, Szewczuk-Karpisz K, Siryk O, Samchenko Y, Derylo-Marczewska A, Kernosenko L, et al. Structure and thermal properties of acrylic copolymer gels: effect of composition and cross-linking method. *J Therm Anal Calorim*. 2024, 149(17):9057–72.

33. Tilghman RW, Cowan CR, Mih JD, Koryakina Y, Gioeli D, Slack-Davis JK, et al. Matrix Rigidity Regulates Cancer Cell Growth and Cellular Phenotype. Hotchin NA, editor. PLoS ONE. 2010, 5(9):e12905.
34. Tusan CG, Man YH, Zarkoob H, Johnston DA, Andriotis OG, Thurner PJ, et al. Collective Cell Behavior in Mechanosensing of Substrate Thickness. Biophys J. 2018, 114(11):2743–55.
35. Wan KY, Jékely G. Origins of eukaryotic excitability. Philos Trans R Soc B Biol Sci. 2021, 376(1820):20190758.
36. Zanutelli MR, Goldblatt ZE, Miller JP, Bordeleau F, Li J, Vanderburgh JA, et al. Regulation of ATP utilization during metastatic cell migration by collagen architecture. Garcia AJ, editor. Mol Biol Cell. 2018, 29(1):1–9.
37. Zhang J, Hochwald SN. The role of FAK in tumor metabolism and therapy. Pharmacol Ther. 2014, 142(2):154–63.
38. Zhang Q, Gu X, Yu Z, Liang J, Dong Q. Viscoelastic Damage Characteristics of Asphalt Mixtures Using Fractional Rheology. Materials. 2021, 14(19):5892.
39. Zhou H, Liu R, Xu Y, Fan J, Liu X, Chen L, et al. Viscoelastic mechanics of living cells. Phys Life Rev. 2025, 53:91–116.